

Dynamic Visualization of Lung Sounds with a Vibration Response Device: A Case Series

R. Phillip Dellinger^a Joseph E. Parrillo^a Alon Kushnir^b Marcello Rossi^c
Igal Kushnir^b

^aDivision of Cardiovascular Disease and Critical Care Medicine, UMDNJ – Robert Wood Johnson Medical School at Camden, Cooper University Hospital, Camden, N.J., USA; ^bDeep Breeze Ltd., Or Akiva, Israel; ^cFisiopatologia e Riabilitazione Respiratoria, Azienda Ospedaliera Universitaria Senese, Siena, Italy

Key Words

Acoustic mapping · Acoustic imaging · Lung ventilation · Pulmonary imaging · Respiratory sounds

Abstract

Background: The field of computer-assisted mapping of lung sounds is constantly evolving and several devices have been developed in this field. **Objectives:** Our objective was to evaluate a new computer-assisted lung sound imaging system, 'vibration response imaging' (VRI), that records and creates a dynamic image of breath sounds. We postulated that the VRI display format would qualitatively and quantitatively reveal breath sound distribution throughout the breathing cycle. **Methods:** Lung sounds were recorded from 5 healthy adults and 14 patients with various respiratory illnesses using VRI. The lung sounds were processed by the VRI software, which incorporates an algorithm to convert breath sounds in the frequency range of 150–250 Hz to a dynamic image and quantitative assessment of breath sound distri-

bution. **Results:** Images and quantifications from recordings of the healthy adults showed distinct patterns for inspiration and expiration. Images and quantifications from the subjects with respiratory illness differed substantially from the images of the healthy subjects. Both healthy and pathological subjects presented some expected characteristics of breath sound distribution. **Conclusions:** The VRI device may provide a new perspective in acoustic imaging and quantification of breath sounds by adding aspects of time analysis and quantification of distribution to existing methods. Further studies will be required in order to establish reliability of repeated recordings and to validate the sensitivity of the system in detecting various lung pathologies.

Copyright © 2007 S. Karger AG, Basel

Introduction

Since the invention of the stethoscope, physicians have routinely listened to the sounds produced by a patient's internal organs, such as the heart and lungs, as an aid in diagnosis and treatment of various disorders. The diagnostic accuracy of the acoustic information, however, is often poor and discrepancies may exist between the stethoscope and radiograph findings. One reason for the low diagnostic accuracy is substantial variability among

R.P.D. and J.E.P. have a consultant agreement with Deep Breeze that includes honoraria and stock options (no current monetary value). I.K. and A.K. are employees of Deep Breeze. Research personnel and materials for the VRI research program at Cooper University Hospital are partially funded by Deep Breeze.

KARGER

Fax +41 61 306 12 34
E-Mail karger@karger.ch
www.karger.com

© 2007 S. Karger AG, Basel
0025-7931/07/0000-0000\$23.50/0

Accessible online at:
www.karger.com/res

Igal Kushnir, MD
Deep Breeze Ltd.
2 Hailan St., P.O. Box 140
North Industrial Park, Or Akiva, 30600 (Israel)
Tel. +972 4 626 6650, Fax +972 4 626 6653, E-Mail Igal.Kushnir@deepbreeze.com

independent observers for the presence of respiratory signs using a stethoscope [1, 2]. Computer-based lung sound technology was developed to evaluate the acoustic properties of respiratory sounds and to provide objective measurements that may circumvent the shortcomings of clinical auscultation. Advances in computer technology made it possible to capture, store, analyze and communicate thoracic sounds that are normally heard through the stethoscope [3]. Acoustic imaging software provides a more complete and less subjective assessment of pulmonary function than auscultation [4].

Many different types of sensors, sensor-coupling methods and digital signal processing techniques have been established for the investigation and analysis of respiratory sounds [5–7]. The acoustic output is usually in graphic or numeric form [5, 7]. Kompis et al. [8] developed an acoustic imaging method that went beyond the graphic and numeric modes of presentation of lung sounds. Based on the knowledge that thoracic sounds are known to contain spatial information, the investigators used simultaneous multimicrophone recordings to assess the spatial information. Graphic representation of the data array was presented as a static, reconstructed, three-dimensional distribution with gray scale coding. According to these investigators, the imaging algorithm could be used to produce real-time imaging, which would open new diagnostic possibilities due to the dynamic nature. However, due to the imaging algorithm running on non-specialized computer hardware, the computation load was too high for such an application. More recent work by Charleston-Villalobos et al. [9] addressed the issue of low spatial resolution in previous studies of lung sound intensity mapping. These authors evaluated deterministic interpolating functions in generating acoustic thoracic images with higher spatial resolution.

We evaluated a computer-assisted lung sound imaging and quantification system that is similar in nature to those reported in the literature, but with variations in system design and in feature extraction and visualization. The dynamic, acoustic imaging algorithm was developed in order to process multisensor signals and to generate a dynamic representation of breath sound distribution, using gray scale coding. Breath sound information obtained with the evaluated device is recorded and saved. The dynamic nature of the image may broaden its clinical value, as it provides continuous visualization of breath sound information along the entire breathing cycle and detailed information about breath sound timing between the different lung locations. Another output of the system that was examined is quantification of region-

al distribution of breath sounds, which is based on the same input as that of the imaging algorithm, but does not contain the timing aspect. The output is a table of percentages of the relative intensity of lung sounds for different segments of the lungs gathered from the entire recording duration.

We postulated that the vibration response imaging (VRI) display format would qualitatively and quantitatively reveal breath sound distribution throughout the breathing cycle. To confirm this hypothesis, we conducted a preliminary clinical assessment in the form of a case series to evaluate breath sound images and quantification in healthy subjects and in patients with various respiratory conditions, and then compared the findings to known and reported breath sound characteristics.

Materials and Methods

Subjects

In order to evaluate the computer-assisted breath sound imaging and quantification system, we studied a case series of 14 subjects with various physician-diagnosed respiratory illnesses and 5 healthy subjects. Subjects were enrolled from 5 different institutions (see Acknowledgments); institutional review board approval for the study was received from each of the institutions. A similar study protocol with the same detailed recording procedure was used at each of the study institutions. The distribution of patients was as follows: 3 males and 1 female (age range 66–75 years) with pleural effusion (fluid volume ranging from 700 to 2,300 ml); 1 male and 3 females (age range 24–75 years) with unilateral central airway obstruction (baseline FEV₁ 24–71% predicted); 1 male and 2 females (age range 19–37 years) with acute asthma attack, expiratory wheezes were identified by auscultation in all 3 cases (baseline FEV₁ 34–70% predicted); 2 mechanically ventilated subjects (a 65-year-old male with atelectasis on pressure support ventilation and a 74-year-old female with pleural effusion on pressure controlled ventilation) who were clinically able to be seated during recordings; an 11-year-old boy with a 5-day obstruction of the left main bronchus due to foreign body aspiration. Healthy subjects were nonsmokers with no history of significant respiratory or cardiac illness; they had been free of respiratory disease or symptoms for at least 1 month before the study. They had normal chest radiograph and spirometry results. Informed consent was obtained from all subjects (and the parents in the case of the child).

VRI Device

Technology

The VRlxp system (Deep Breeze Ltd., Or-Akiva, Israel) is a computer-based lung sound recording, imaging and quantification system. Like other equipment specifically designed for the analysis of respiratory sounds, development of the VRlxp System was based on several concepts regarding the generation and processing of breath sounds. It is presumed that breath sounds are

Fig. 1. Schematic diagram showing the 5 main components of the VRI device: sensor matrix array of 40 sensors; vacuum unit; hardware board including preamplifier and A/D converter; PC and imaging and quantification software; algorithm.

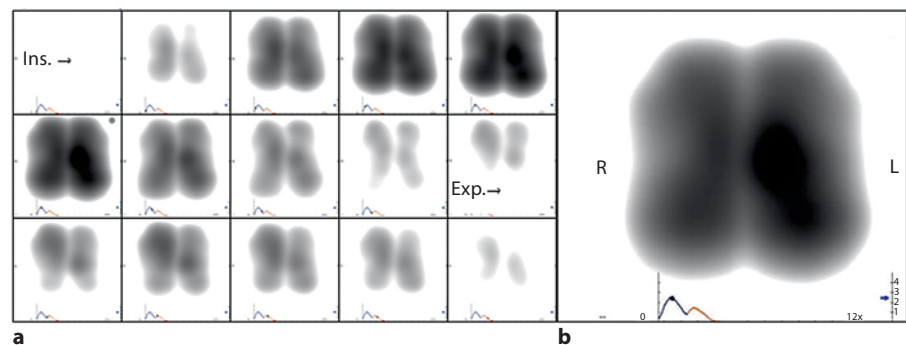
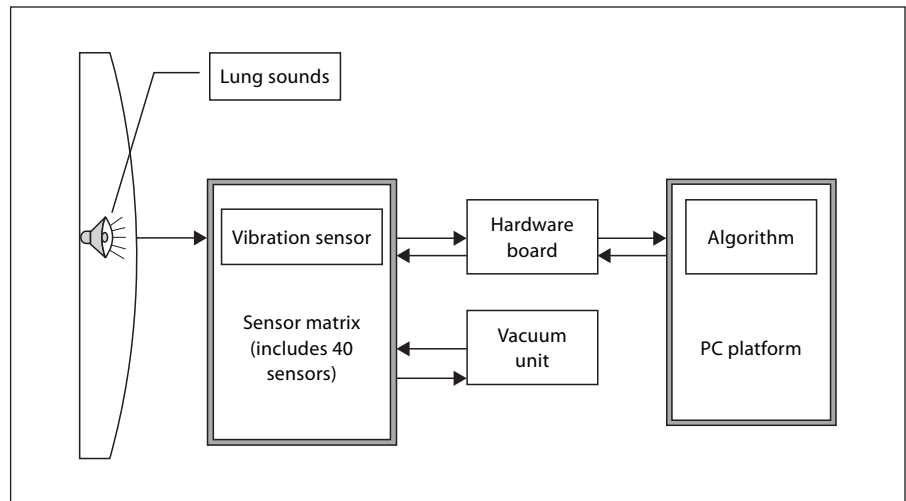


Fig. 2. Example of a VRI image of a normal subject. **a** Sequential frames, beginning with inspiration (from the upper left-hand corner moving across in a left-to-right direction, frames 1–9), are sliced over time intervals of 0.17 s, which comprise a VRI dynamic image and reflect regional vibration properties along time; **b** Maximal Energy Frame of a VRI dynamic image (the x-axis in

the graph represents the time of recording in seconds and the y-axis represents average vibration energy from all 40 sensors, as calculated in Appendix 1). In this case, 1 respiratory cycle is presented, which contains approximately 1.5 s of an inspiratory phase (first waveform in graph; black dot represents peak inspiration) followed by 1.5 s of an expiratory phase (second waveform).

generated by turbulent air and vibrations within the lungs and its airways [10]. As airflow in the large and medium-size airways reaches a critical velocity, it induces turbulence. The vibrations are affected by the structural and functional properties of the lungs and can exhibit responses that may vary in frequency, intensity, space and time. The resulting sound energy, from the turbulent air and vibrations, is transmitted to the skin, after filtering by the lungs and chest wall [7, 10]. Breath sound amplitude differs between different locations on the chest surface, with different patterns for inspiration and expiration, and between persons [7]. While the heterogeneous distribution of breath sound amplitude is not completely understood, these variations have been described in detail and particular patterns have been documented [7].

The VRI device captures the image of the lungs by recording the energy generated by the vibrations of the lungs during both inspiratory and expiratory phases of breathing. The vibrations are discerned by 2 arrays of piezoelectric sensors. The sensors' signals

are transferred to a hardware board and are processed by the VRI software (fig. 1). Although there are known algorithms for processing multimicrophone signals [8], the algorithm that was developed for the VRI device is unique, as for the first time (to our knowledge) vibration energy is converted to a sequence of dynamic images (fig. 2a) that reflect regional vibration properties. The output signals from a bank of bandpass filters are combined and sliced over regular time intervals (0.17 s). The output is not expressed in terms of decibels, but as an image of relative intensities of breath sounds between different locations in the lungs along time. The vibration energy can also be analyzed regionally (in percent) for upper, middle and lower zones of both the right and left lung. In addition, the total output from all the sensors is presented as an intensity bar and graph over time, which is used only as reference for general estimation of the timing of the recorded sounds. Any change in frequency, intensity, space and timing of the airflow that affects the lung vibration response

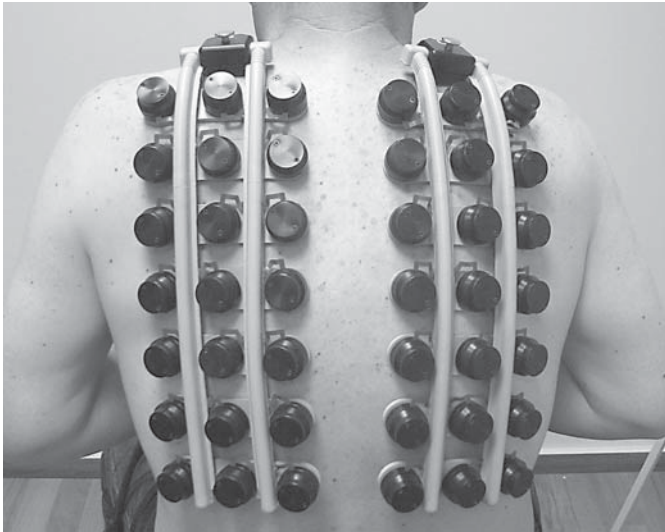


Fig. 3. Forty active piezoelectric contact sensors and 2 inactive contact sensors (on the left and right peripheries of the first row) are assembled on 2 planar arrays and are adhered, by a constant computer-controlled vacuum method, on each side of the subject's back to cover both lungs.

should be reflected in the image and in the regional quantification. Structural alterations, such as space-occupying lesions, and functional alterations, such as bronchial obstruction and chronic obstructive pulmonary disease, can modify the vibration response.

Sensor Technology

Forty active piezoelectric contact sensors and 2 inactive contact sensors (left and right peripheries of the first row; Meditron ASA, Oslo, Norway) with a linear frequency response of ± 2 db in the frequency range of 50–400 Hz are assembled on 2 planar arrays and adhered to the posterior chest on each side of the subject's back to cover both lungs (fig. 3). This type of sensor is used in the Welch Allyn electronic stethoscope and, as such, has been tested for reliability and stability by the manufacturer and in the field. Furthermore, the VRI device has work specifications of 15–35°C and storage specifications of 1–60°C, which ensures repeatability and stability of all device elements.

The distance between the centers of the sensors is uniform throughout at 5 cm in each array. Each row of 3 sensors within these 2 VRI sensor arrays (V-arrays; left and right side of the chest) is held in place by a silicone cup that is coupled to the back by a computer-controlled low vacuum. The vacuum pressure is maintained constant, ensuring ease of attachment. This method is used in order to address the issue of applying 40 sensors with a specifically controlled pressure and defined location, while accommodating individual human anatomical variability. The accumulation level of the vacuum system is discerned and controlled by the VRI software.

Various sized V-arrays for adult males, adult females and children are being developed according to average thoracic height and lateral dimensions. The distance between the center of the

sensors and the total number of sensors determines the dimensions of those V-arrays. The adult V-array contains 40 sensors and the pediatric V-array contains 34 sensors.

Noise-Filtering and Data-Acquisition Technology

The VRI device utilizes several stages of filtering to select a specific frequency band. The filtering is also used to reduce distortion and interference (such as background noise and undesirable signals coming from the heart and muscle) and to enhance the signal by reducing all other frequency components that may be present in the noisy signal. The filtering process includes: bandpass filtering (150–250 Hz) that allows only the desirable frequency range of breath sounds [11] and reduces interference generated by chest wall movement and heart sounds [8]; median filtering which suppresses impulse noise; truncation of samples above a given threshold. Subsequently, singular value decomposition is used to identify only meaningful underlying variables.

The limited frequency of 150–250 Hz is appropriate for capturing breath sounds, while filtering heart sounds. Other bandpass filtering, such as a range of 350–850 Hz for crackles and 100–800 Hz for wheezes can be applied by additional VRI algorithms to digitized sound signals when examining abnormal lung sounds. The scope of the present study was limited to distribution of breath sounds; algorithms for abnormal lung sounds were not investigated.

A special 64-multichannel analog-to-digital converter was developed for data acquisition, which enables filtering the sounds, amplifying the signal and converting the analog signal into digital data. The system includes a 16-bit acquisition level [5] and a sampling rate of 19.2 kHz [5] that acquires the analog signals and converts them to digital data, which are displayed on the VRI computer platform. In addition, there is a low-noise preamplifier on each sensor. The preamplifier purpose is to amplify the signal coming from the sensor and to prevent interference, which might otherwise be induced on the signal along the cable.

The Algorithm and Software

The VRI algorithm combines the filtered output signal frequencies to assemble a gray scale-coded dynamic image. A detailed description of the algorithm is provided in Appendix 1. The gray scale pattern represents the data signals (vibration field coordinates) at each sensor position. Creation of the gray scale pattern involves the following steps. Bandpass filtering of 150–250 Hz is applied to extract the desired lung sound data. The resulting signal, for each sensor, is downsampled to produce envelope (EVP) signals, which are correlated with the respiration cycle. These EVP signals are then converted into a logarithmic scale:

- Refer to the back as an XY plane and let $EVP(x_i, y_i, t)$ ($1 \leq i \leq$ number of sensors, $0 \leq t \leq T$) represent the EVP sample t of the sensor located on the back at (x_i, y_i) .
- For each time slot, t , we assemble a plane in which the (x_i, y_i) position equals $EVP(x_i, y_i, t)$.
- Since the positions of the sensors are discrete, a two-dimensional interpolation is exercised, using a Gaussian interpolator.

The gray scale-coded dynamic image of the lungs is then created from the series of the planes.

The output is a dynamic image of a two-dimensional coordinate system. High data areas where lung vibration energy is greatest are depicted as dark colors (black) and low data areas are shown

in light colors (light gray); the minimum data area is defined as 'white'. Each subject's recording (12 s) has different high- and low-value areas within each respiratory cycle, according to the vibration intensity. The high and low values are always determined as black and white, respectively; thus, each recording is normalized to these values. Two-dimensional graphical representation of the average vibration energy is converted into an image that may be analyzed by an interpreter, in a similar manner to the analysis of images obtained by other methods such as a radiography or ultrasound. The imaging algorithm will create some sort of image from any input by detecting a maximum point and a minimum point and adjusting the gray scale distribution according to the input from all 40 sensors. Therefore, even attaching the sensors to an inanimate object such as a table surface will create an image. However, since the sensors are directional, they record the dominant input signals. When the sensors are attached to the back of a subject, while breathing and not breath holding, the breath sound signals have a very high signal intensity compared to any background noise, and therefore these sounds will be the dominating input in the gray scale distribution. Any background noise will be defined as white regions in the image. Furthermore, not only are the gray scale distribution and dynamic development irregular in recordings of inanimate objects, but also the contour of the image is atypical and does not resemble the shape of the lungs.

The overall time of a respiratory cycle may be divided into a variety of intervals with each interval representing the total vibration energy accumulating over that time period. Images attributed to each interval may then be displayed sequentially on the displayed device representing the regional distribution of vibration (fig. 2a). This generates a movie that shows dynamic changes occurring in the vibration energy throughout various lung regions, over the time interval, whereas the gray level scale enables following the course of the dynamic development of the lung vibrations in the image.

As peak flows are not identical from one breath to another, the computer measures the maximum vibration energy during inspiration and uses this value for normalization of the image (Appendix 1). This segment is referred to as the maximal energy frame (MEF). The MEF (fig. 2b) approximates peak inspiration and can be used for comparison of different breathing cycles. Static MEF figures, as shown in this study, are the most suitable form for displaying the data in a nondigital form; however, evaluation of the dynamic image is crucial for analysis of lung images. Frame-by-frame development of the image during inspiration and expiration, as well as variations between the 2 phases, provide additional information regarding lung sound distribution.

In addition, a graph is produced that represents the average vibration energy units, gathered from all 40 sensors, as a function of time. This graph appears under the image and serves the purpose of providing general timing information (within the breathing cycle). The graph does not provide data on decibel values. The user is able to select any point along the graph in order to view a static image of the vibration energy at that particular point of inspiration or expiration.

Quantitative Regional Assessment

VRI displays the percentage contribution of each lung to the total vibration signal. The VRI device acquires the signal data for all 12 s of recording, and the algorithm extracts the relative energy level of each lung out of the total (100%) lung vibration. Each

	Right (%)	Left (%)
Upper	7.56	11.92%
Middle	20.63	23.34%
Lower	17.22	19.34%
Total	45.41	54.59%

Fig. 4. Table of percentages for regional assessment of vibration energy in a healthy subject. Fractions of the total VRI energy units for each corresponding regional signal are divided into 3 regions for each lung.

total lung percentage is calculated from the corresponding sensor matrix, which contains 7 rows of 20 sensors (in the upper row, the peripheral sensor was not used). Each lung can then be further partitioned into 2 or 3 different regions, according to the user's preference. In this report, division of lung segments was based on 2 upper rows, 3 middle rows, and 2 lower rows. The fraction of the total VRI energy units for each corresponding regional signal is displayed in a table of percentages (fig. 4). Appendix 1 shows the mathematical equations (1–3) that are performed in order to calculate the results which are used to determine the relationship (in percentages) between the different zones.

Recording Procedure

Subjects were recorded in a quiet, but not soundproof, environment. The V-array was placed on the subjects' backs as follows: (1) the upper row of each array was 2 ± 1 cm above the scapula, (2) the inner sensors of the upper rows were 5 ± 1.5 cm from the vertebral column, and (3) the bottom rows of the 2 arrays were at approximately the same height (within ± 1.5 cm; fig. 3). In order to ensure proper attachment and prevent artifacts, the sensors should not be placed on the spine or scapula. It is not necessary to attach the sensors in identical locations for repeat measurements; however, the sensors should be placed as described above and with particular attention to the bottom row. A considerable difference in row height between the left and right arrays will be reflected in the image (i.e. the bottom of one lung will be lower than the other lung). The V-array was then coupled to the back by a computer-controlled low vacuum method. Ambulatory subjects were seated and instructed to take normal, deep breaths through the mouth during image recording. No forced exhalation or other breathing maneuvers were performed. The breathing volume, flow and timing were not documented by spirometry during the recording. We found breathing through a spirometer while recording to be cumbersome for the subjects and the operator, thereby affecting the practicality of the device. In order to attain a level of standardization of the subjects' breathing intensity and breathing rate, subjects received feedback information from the VRI intensity bar and breathing graph. The subjects were instructed to target their breathing to a range of 1.5–3.5 on the breathing intensity bar and

to a breathing cycle rate of 18–24 cycles per minute. This established a relatively consistent breathing pattern between recordings and between subjects. Additionally, 2 recordings were performed for each patient. Although the study is limited by the lack of precise standardization of breathing volume and flow, each recording contained 3–4 breathing cycles and each patient had 2 recordings, resulting in 6–8 breathing cycles per patient per subject. By comparing the findings of the readers and the quantitative output, no significant differences were observed. A study to determine the boundaries of breathing parameters that will result in similar VRI output is being conducted. The process is also suitable for the pediatric population and does not require considerable patient effort. Respirations were recorded within a period of 12 s, which is generally 3–4 breathing cycles in healthy individuals. In bedridden patients, including mechanically ventilated patients, the head of the bed was raised to 60° and the patient was held, by trained personnel, in an upright position during the recording.

For practical purposes it is not possible to conduct recordings in clinical settings that eliminate all environmental noise; therefore, it is likely that occasionally artifacts will be encountered in recordings. Artifacts not filtered by the software were found to be easily identified in the image, and the environmental source of the artifacts was usually recognizable upon listening to the recordings. For the purpose of this study, all recorded segments with artifacts were marked for exclusion from further analysis.

Image-Reading Procedure

A standardized evaluation form was developed in order to assess the various characteristics of the VRI image. The purpose of this tool was to ensure consistency of image analysis. A panel of 2 pulmonologists and 1 radiologist, familiar with VRI images, were instructed to document their observations of both dynamic and static images according to the following parameters: (1) general appearance of the full dynamic image, which consists of a gray scale representation of the data signals for the entire 12 s of recording; (2) frame-by-frame evaluation of image development from frame 1 to the MEF, which is a representation of a 0.17-second segment of the recording during inspiration in which gray scale distribution of the lungs is at the maximum and data values are the highest; (3) evaluation of the MEF in terms of shape, right versus left lung symmetry and right versus left vibration energy; (4) evaluation of missing areas, defined as areas in which data signals are absent (white points in gray scale coding) from the image though signals are generally present in that area. Any disagreement among the 3 image-analyzing physicians was adjudicated. The images were then compared to existing standard imaging and lung function technologies such as chest radiographs, perfusion scintigraphy, computed tomography and pulmonary function tests. Any existing common characteristics for the various lung conditions were documented.

Results

All 28 VRI procedures (14 patients) were conducted in a standard clinical setting. All procedures took less than 2.5 min on average, from the time of system operation to the time of data presentation (adherence of sensors \pm 1

min; recording duration 12 s; image display 15 s; quantitative data display 20 s). Reading of the VRI images took 3.5 min on average, including completion of the standard interpretation form. The sensors were adhered to the posterior chest in the defined locations (\pm 1.5 cm) of all patients, and there were no reports of adverse events or difficulty in adherence procedure. None of the subjects reported discomfort from adherence of the multiple sensors.

Healthy Subjects

VRI dynamic and MEF images of 5 healthy subjects were evaluated for common features. The breathing patterns of the 6–8 cycles in each of the 2 recordings and between the 2 recordings for each healthy subject did not show notable differences, according to qualitative assessments. The difference in quantitative assessments between the 2 recordings of each patient was $<1.5\%$ between corresponding lung regions. Readily identifiable features were common among the images of the healthy subjects. The dynamic image showed both an inspiration phase and an expiration phase. These phases were also reflected in the vibration response graph below the image. The horizontal axis of the graph is a time axis of the 12-second recording period, while the vertical axis represents average vibration energy units. Both the inspiration and expiration phase of the continuous dynamic image had a progressive and regressive appearance. There were differences, however, between the 2 phases of respiration. Inspiratory vibration energy was higher than expiratory energy (also demonstrated by the line graph beneath the VRI image). Additionally, in 3 of the 5 healthy cases, the gray scale intensity in the image was slightly greater in the left lung during inspiration and slightly greater in the right lung during expiration.

The dynamic image, comprised of the left and right lungs, developed bilaterally in a similar, yet not identical, manner. Vertical movement of gray level-coded signal distribution and intensity was discernible. The MEF image (fig. 2b) shows the maximum area of the vibration distribution (anatomically resembling the lungs) and is distinguishable from other still frames. The MEF images of the 5 healthy subjects had similar contours, a comparable number and location of energy centers, and similar gray level distribution of vibration response, although slight differences were noted between subjects. The contour was lobar with narrowing towards the top and slight widening in the lower lung regions below the midsection. Two to 3 vibration energy centers with higher signal intensity appeared along the upper and lower regions of each lung. A vertical stripe was observed between the

lungs, corresponding to the area of the spinal column in which sensors were not attached. The vertical stripe was an expected feature, as there is no sound input to the imaging algorithm in this area.

All VRI viewers reported that the lung vibrations from the start of inspiration to MEF (between 4–6 frames in the VRI dynamic image, which is equal to approximately 0.7–1.2 s) gradually increased from the upper third part of the image toward the peripheries, mostly towards the lower part of the image, until the vibration response was distributed to its maximum area. There was similar development of the right and left lungs during this phase of respiration. From the MEF to the end of inspiration (between 3–5 frames in the VRI dynamic image, which is equal to approximately 0.5–0.9 s), all reviewers reported gradual decrease from complete distribution of vibration energy to a reduced response, transpiring in the direction of the lower regions towards the upper part of the image. Movement was opposite that of dynamic development in the first phase of inspiration; however, dynamic distribution of vibration energy also demonstrated bilateral symmetry during this breathing cycle phase.

The regional quantitative assessment of the 5 healthy subjects showed noticeable similarities in distribution of the energy. The vibration energy was concentrated primarily in the middle and lower regions with less energy in the upper lungs. This corresponds to the descriptions of features in the images of the healthy subjects. Higher values of vibration energy were computed for the total left lung (mean vibration response $54.4 \pm 2\%$; range 51.35–56.94%) in comparison to the total right lung (mean vibration response $45.6 \pm 2\%$; range 43.06–48.65%). Although the sample size is small, the values for the left lung were frequently higher than those for the right lung. The vibration energy of corresponding regions of the right versus the left lung differed by an average of $1.05 \pm 1\%$ for the lower region, $2.37 \pm 0.4\%$ for the upper region and $5.6 \pm 1.8\%$ for the middle regions. There was less variation among subjects when comparing the total values for the right or the left lung than when comparing the right versus the left lung within a subject. Figure 2b shows a VRI image of a healthy subject with the graph of average vibration energy below the image. Regional quantitative assessment of this image is presented in a table of percentages (fig. 4).

Subjects with Lung Pathologies

In general, structural and functional changes in the lungs that alter the breath sounds change the intensity, distribution, dynamic symmetry and dynamic move-

ment of the VRI image when compared to the healthy images. The features that were described as abnormal and corresponded with various lung pathologies included the following: localized or overall reduction in the vibration response; tapering or thinning of the overall lung image with lack of data signals around the periphery; disturbances in the progression of the dynamic image; lung regions with no vibration signals; asymmetry between the right and left lungs; irregular contour in the MEF; general distortion of the image.

Pleural Effusion

VRI images of the 4 ambulatory patients with pleural effusion demonstrated asymmetrical expansion of the lungs with reduced vibration response and lagging expansion on the affected side. Narrowing of the lung image with significant tapering of energy distribution was observed in the area of the effusion during all stages of the breathing cycle. Furthermore, there were areas in the lower lungs with very low vibration distribution or without vibrations that created a very distinct triangle shape in the image (fig. 5a), corresponding to the location of accumulated fluid on chest radiograph. On auscultation of the chest, no bronchial sound was found on the site of pleural effusion in all 4 patients. The regional assessment value for the lower left lung was 4.83% for 1 case of left-sided effusion (compared to the average $20.1 \pm 3\%$ for lower left lung in healthy subjects) and 1.76–6.51% for 3 cases of right-sided effusion (compared to the average $19 \pm 2\%$ for lower right lung in healthy subjects). The size of the effusion was associated with the reduction in the vibration response such that larger effusions resulted in lower percentage values for regional assessment in that region and in the overall lung. Following drainage, both the VRI images and the chest radiographs showed improvement. In one case of right-aided pleural effusion, regional quantitative assessment showed that distribution of the energy in the affected lung differed from right lung distribution in the healthy subjects. The vibration response in the lower lung region was reduced (6.51% vs. $19 \pm 2\%$ in healthy subjects). After drainage, the response in the lower right region of the VRI image increased considerably (fig. 5b). Regional assessment in this area also demonstrated an increase to an almost normal value of 15.4%.

Central Airway Obstruction

VRI images of the 4 patients with central airway obstruction showed considerable reduction in the overall vibration response of the obstructed lung during all phases of respiration. Whereas pleural effusion resulted in a lower

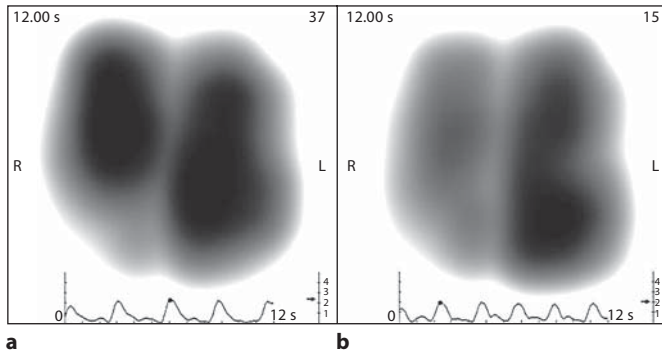


Fig. 5. MEF images of a female patient with pleural effusion of 700 ml in the right lung. **a** MEF before drainage shows a lack of vibration response that created a triangle shape in the lower right lung, corresponding with the location of accumulated fluid on chest radiograph. **b** After drainage, the response in the lower right region increased considerably.

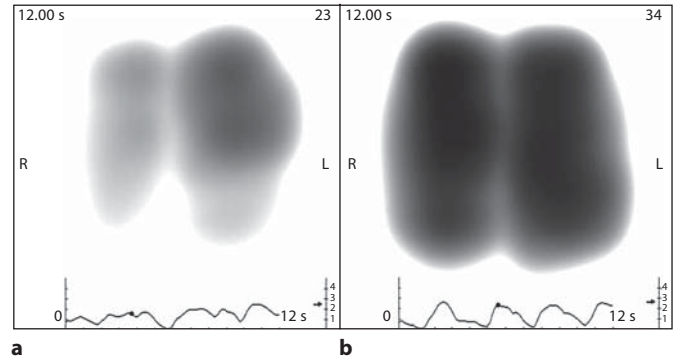


Fig. 7. MEF images of an acute asthmatic patient. **a** Before bronchodilation, the VRI image showed intense vibration in the upper left lung and an overall reduction in vibration energy in the remaining areas of the left lung, as well as reduction in the right lung. **b** Following bronchodilation and an increase in FEV₁ of 18%, the VRI image showed improvement in the asymmetrical distribution of energy, similar to that of a normal subject.

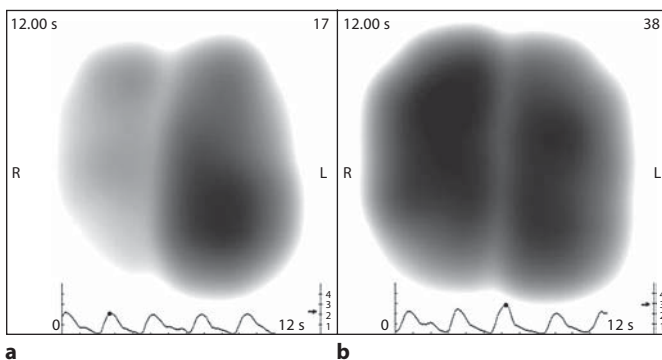


Fig. 6. MEF images of a 74-year-old male with airway obstruction (stenosis at right main bronchus by granuloma). **a** Prior to intervention, the image showed an overall reduction in vibration response in the right lung. **b** After balloon dilation and laser resection, the VRI image showed a significant increase in vibration response in the obstructed lung.

vibration response in the area of accumulated fluid (right or left lower lung), central airway obstruction resulted in an overall (total lung) reduction in vibration response in the obstructed lung. Following intervention (after 4 h), the vibration response increased considerably in the obstructed lung. Success of interventional outcome was measured by bronchoscopy, spirometry and clinical status.

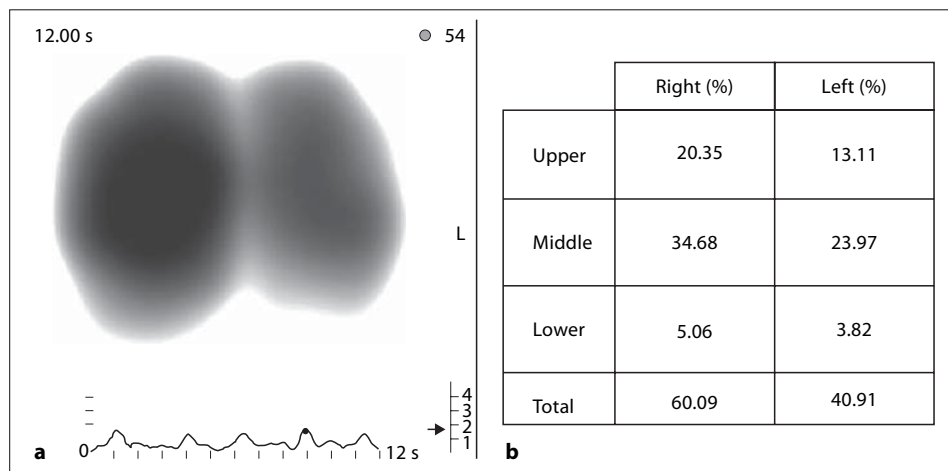
This image vibration reduction was also noted in the quantitative regional assessment of the total lung that was obstructed. Figure 6a demonstrates the case of a 74-year-old male with airway obstruction (stenosis at right main

bronchus by granuloma), in which there was a diminished vibration response in the right lung. After balloon dilation and laser resection, the VRI image showed a significant increase in vibration response in the obstructed lung (fig. 6b). Regional assessment for the total right lung in this patient increased from 26% at baseline to 48% after the operation.

Acute Asthmatic Attack

VRI images for 3 acute asthmatic patients showed a markedly asymmetrical distribution of vibration energy prior to bronchodilation. The asymmetrical patterns with changing distribution were observed throughout the breathing cycle pattern. Although hypervibration in the upper left lung was observed in 1 case during inspiration, there was an overall reduction in vibration energy in this image during inspiration (fig. 7a). Expiratory vibration energy was greater than inspiratory vibration energy in the VRI graph, which was a reversal of the graph pattern observed in healthy subjects. In 2 cases, 1 lung showed considerable reduction in energy compared with the other lung. Following bronchodilation (salbutamol) and an increase in FEV₁ of at least 10%, VRI viewers documented improvement in the asymmetrical distribution of energy in the images and in the graph pattern for all 3 patients (fig. 7b). These images were defined as normal (similar to those of healthy patients) in 2 of the 3 cases. Regional assessment quantification for the 3 patients did not correlate with the VRI image findings or clinical assessment of the patients.

Fig. 8. MEF image of a mechanically ventilated patient with left lung atelectasis. **a** The VRI image shows a reduction in total lung vibration response in comparison to nonventilated patients. **b** Regional quantitative assessment shows very low values in both lower lungs (left lower lung 3.82% and right lower lung 5.06%) compared to values for normal subjects (left lower lung 20% and right lower lung 19%).



Mechanically Ventilated Patients

VRI images of patients on mechanical ventilation with pleural effusion and atelectasis showed VRI image features similar to those of nonventilated patients with lung pathologies. The readers observed that the total lung vibration response appeared to be reduced in the image in comparison to nonventilated patients. Regional quantitative assessment, in a patient with lower lobe atelectasis, showed very low values in both lower lungs (left lower lung 4% and right lower lung 5%), compared to values for normal subjects (left lower lung 20% and right lower lung 19%). Figure 8a and b shows the VRI image and the regional assessment of this subject. In the patient with pleural effusion of the right lower lung, the values for the lower and middle regions of the right lung were mildly reduced: right lower lung 16% and right middle lung 13%, compared to an average of 19 and 19.7%, respectively, of healthy subjects.

Foreign Body Aspiration

The VRI image of a child (11-year-old male) with a foreign body completely obstructing the left main bronchus (diagnosed by bronchoscopy) showed extensive reduction of vibration energy in the left lung (fig. 9a). Regional assessment confirmed that the left lung contributed to only 9.8% of the total vibration energy. Abdominal and chest radiographs were reported as normal, physical examination revealed decreased breath sounds over the left hemithorax. Following rigid bronchoscopy to remove a plastic pen cap in the left main bronchus, a follow-up VRI image showed marked augmentation of the vibration response of the left lung to a nearly normal state (fig. 9b). Regional assessment of the vibration response in

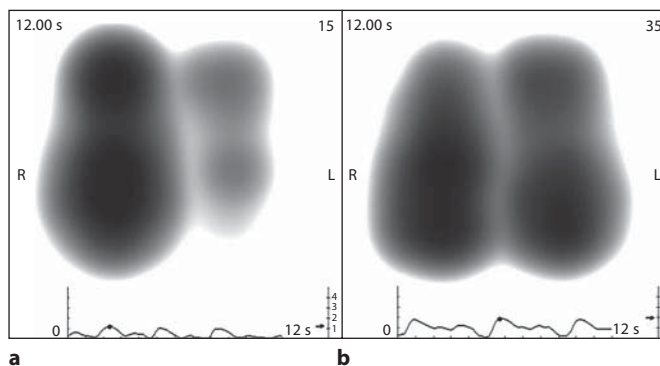


Fig. 9. MEF image of an 11-year-old male child with a foreign body completely obstructing the left main bronchus. **a** Prior to foreign body removal, the VRI image showed extensive reduction of vibration energy in the left lung. **b** Following rigid bronchoscopy to remove a plastic pen cap in the left main bronchus, a follow-up VRI image showed marked augmentation of the vibration response of the left lung to a nearly normal state.

this patient changed from 9.8% in the left lung and 90.2% in the right lung at baseline to 57% in the left lung and 43% in the right lung after bronchoscopy.

Discussion

In this case series, we validated various characteristics of breath sounds from VRI images of both healthy subjects and subjects with various lung pathologies. The present findings suggest that visual representation and regional assessment of breath sounds data is feasible, both qualitatively and quantitatively.

In healthy subjects, images produced during inspiration showed typically higher levels of breath sounds (vibration energy in the VRI) compared to expiration. This observation is similar to other reported findings [12]. Completely uniform distribution of vibration energy within each lung was not observed in any of the images, as expected due to the structure of the lungs. The tapering of the image in the upper lung regions was compatible with attenuation of vibration energy in this area, as compared with the lower lung regions. The contour in the upper region was affected in part due to the 2 inactive sensors on the peripheries of the upper row of sensors. However, the difference in intensities between regions does not rely on the number of sensors, but rather on the intensity of the signals that are recorded. This is further demonstrated by differences in the average distribution of vibration energy. Corresponding regions of the right versus the left lung differed by an average of $5.6 \pm 1.8\%$ for the middle regions (both right and left lungs are recorded by 3 rows of sensors), while the average energy in the right middle region (3 sensor rows) was only 0.77% greater than the average energy in the right lower region (2 sensor rows). This observation is in agreement with findings that breath sounds are not uniform over the lungs and there are regional variations in sound intensity [7]. The finding that vibration energy was higher in healthy subjects in the lower regions than the apex is also in agreement with the work of O'Donnell and Kraman [13], who reported that the amplitude of sound along the posterior vertical recordings tended to be greater in the base than the apex. Additionally, the higher distribution of vibration energy to the lower regions is a gradual process in which the maximum is reached at the midpoint of inspiration. Ploy-Song-Sang et al. [14] also reported that breath sound intensity in the base increased from residual volume to midvital capacity (or up to 60% depending on the positioning of the sensors) and then decreased as total lung capacity was approached.

Pasterkamp et al. [15] reported greater power at left posterior sites (base and superior lung locations) for baseline measurements in healthy controls and in subjects with asthma. Other studies have also observed this pattern of left-sided dominance of lung sound intensity in healthy individuals [16, 17]. The authors stated that the observed asymmetries are likely related to the effects of cardiovascular structures and airway geometry on sound generation and transmission. Our quantitative measurements of VRI regional data of 5 healthy subjects (based on measurements with low frequencies of 150–250 Hz) also showed left-over-right dominance in total lung mea-

surements. While higher values for lung sound intensity in the left lung occurred during inspiration in the previous studies, we must take into account that regional assessment by the VRI algorithm does not distinguish between values for inspiration and expiration. According to the VRI image analysis of the 5 healthy subjects, we postulate that the left-sided dominance arose from higher values during inspiration; however, during expiration, the intensity of the vibration response in the image was observed to be higher in the right lung than the left.

We observed different image patterns for inspiratory and expiratory sounds with an increased vibration response during inspiration compared to expiration. Dosani and Kraman [16] demonstrated amplitude variations between inspiration and expiration. The difference in the distribution pattern between inspiratory and expiratory sounds can be explained by the fact that the inspiratory and expiratory components of normal breath sounds are generated within different locations [7], so the air turbulence and vibrations that generate these sounds will produce different patterns between the 2 phases.

Analysis of the common image features in the healthy subjects provided a reference for comparison with lung pathologies. It is a well-recognized finding that breath sounds are diminished over a pleural effusion. We also observed reduction of vibrations in the image in the areas with accumulated pleural fluid. The area corresponding to the pleural effusion was very distinct on the MEF and appeared as a triangular region with an obvious diminution of signal response. This finding suggests that VRI may provide a tool to quantify regional decreases in vibrations, to compare changes in the measurements during the course of treatment and to improve evaluation of posttreatment lung expansion. Further studies are warranted to correlate the regional vibration decreases with effusion size.

We observed significant changes in the VRI patterns before and after intervention in central airway obstruction. These changes could be quantified by algorithms and, thus, may serve with further investigation as a means for objective quantification of pre- and postintervention status.

Reduction in inspiratory breath sound intensity during induced airway narrowing (asthma) has been reported [15, 16, 18]. While unilateral reduction was reported for 2 cases in our study, the most important observation the VRI reviewers made regarding asthmatic patients was that reduction of vibrations and bilateral asymmetry were not constant at all time points during the breathing cycle. These dynamic changes in vibration intensity

throughout the breathing cycle were very distinct from the patterns exhibited in the dynamic images of healthy subjects. Given that wheezes were identified by auscultation and were present only in the expiratory phase, the findings that were identified in the inspiration phase cannot be explained by wheeze peaks [15]. It is difficult to directly compare our study with previous ones, as the location of recording was limited to the right posterior base in 2 of the studies and the measurements were reported for inspiration rather than as dynamic measurements at various time points during respiration. Although there were no definite findings with quantification of VRI in the 3 asthmatic patients in our study, we believe that a more advanced regional assessment algorithm that would separate inspiration from expiration would provide more informative results.

The reversible increase in expiratory lung sound intensity that we observed has also been reported by Schreur et al. [19] during allergen-induced early and late asthmatic responses in adults. Following bronchodilation, all studies reported an almost complete reversal in reduction changes. We also observed that normal VRI values were restored, resembling a healthy image, and that dynamic irregularities disappeared following bronchodilation.

Use of VRI in mechanically ventilated patients, though limited, demonstrated distribution of lung sound energy with reduction in specific regions. Ploy-Song-Sang et al. [14] showed that breath sounds could be used to measure ventilation of different lung regions. The regional ventilations per unit of volume were similar to data in the literature obtained with radioactive gases. Leblanc et al. [12] also correlated breath sounds with pulmonary distribution. The fact that VRI shows distribution of lung sounds in a rapid manner in mechanically ventilated patients may prove to make it a valuable tool for the assessment of recruitment maneuvers and ventilator adjustment at bedside.

Although there was only 1 case of foreign body obstruction, we did observe a clearly identifiable reduction of vibration response in the left lung throughout the breathing cycle. Regional assessment also demonstrated a severe reduction of vibration energy in the left lung. These findings were compatible with total obstruction of airflow to the left lung, as confirmed by rigid bronchoscopy.

VRI Technology

Our results demonstrate that the VRI procedure, including sensor placement in an accurate manner on var-

ious types of backs, recording period, algorithm calculations and display, was performed in an acceptable time interval. This indicates that the device may have practical utility in a standard patient care setting.

VRI algorithm and display present breath sound distribution in a dynamic gray scale image, a still peak inspiratory image, a graph of average energy, and quantitative data in numerical form (table of regional assessment of vibration energy). This form of presentation, in essence a dynamic map of breath sound distribution, was found to be appropriate for understanding breath sound distribution and timing by the readers, who were not experts in the field of lung sound research. The readers understood the correlation between the images and breath sounds heard with a stethoscope. We did not attempt to correlate distribution of breath sounds with functionality (i.e. ventilation) in this study. Other studies have shown a relationship between breath sound distribution and ventilation distribution [11, 14].

This study focused on a description of the actual observations that were reported for breath sound distribution in a healthy population and in lung pathologies and did not attempt to establish the reliability of these observations. A recent study, conducted at the Royal Brompton Hospital, London [Maher, T, pers. commun., 2006], established the reproducibility of VRI recordings of breath sounds taken from the same individual at different time points. In addition, intra- and interrater agreement on the interpretation of dynamic acoustic lung images of 29 subjects demonstrated a good to very good level of agreement.

In addition to the algorithm and display, another feature of the VRI device is the design of the V-array sensors. Recording of respiratory vibration can be accomplished by either air-coupled microphones or contact microphones. The piezoelectric contact sensor was chosen for the VRI device, since contact sensors are more sensitive and less influenced by ambient noise than air-coupled sensors (condenser microphone): 'Contact sensors discern directly the vibration of the radiating surface and represent a kinematics approach as opposed to the acoustic approach of air-coupled sensors' [20]. 'One of the main problems of contact sensors is the dependence on the force of application on the chest wall, which should be kept constant among different measurements to allow a comparison of data' [20]. This problem was addressed by using a computer-controlled low vacuum method for the coupling of the 2 V-arrays to the back. The adult V-array dimensions were designed according to the average thoracic adult height and lateral dimensions and based on

those previously reported by Bellemare et al. [21]: average thoracic height measurement was 23.3 ± 2.8 cm in males and 22.8 ± 1.9 cm in females, average thoracic lateral measurement was 27.5 ± 1.1 cm in males and 24.9 ± 1.1 cm in females. Given that there are adult individuals and children for whom the standard adult V-array is not suitable, differently sized V-arrays may need to be developed. The distance between the V-array sensors was optimized according to the properties of sound vibration in the human thorax. Thus, the sensors only capture the relatively short wavelengths from inside the lungs and not the long wavelengths of the thoracic cage [3, 22, 23].

Lung sound analysis beyond the stethoscope has always been the domain of highly trained researchers, as the level of sophistication required for the recording and analysis procedure limited use of the technique in practical applications. Other researchers have developed lung analysis tools that can potentially be used in standard clinical practice from a practical point of view – ease of sensor placement [2], data display [2, 9, 15, 24] and detection of abnormal lung sounds [25, 26]. Those devices and the VRI device still require further evaluation regarding aspects of day-to-day practice: ease of use, duration of the overall process, display analysis and reading by non-researchers of lung sounds, and reproducibility and reliability.

Limitations of the VRI technology include a lack of measurement for standardized airflow. There exists the possibility that increased flow or more turbulent flow may produce an increase in vibration energy. Therefore, it is imperative that the image and energy signals are not interpreted in isolation of readily available clinical information. A system for automatic determination of flow is currently being developed in order to address this limitation. In addition, the separate normalization of each image when performing serial imaging studies makes it more difficult to qualitatively analyze serial changes in absolute vibration energy. This can be overcome with quantitative analyses, such as absolute vibration energy units across multiple studies. Also, similar to other imaging systems, artifacts may be produced [23]. Artifacts may appear on the VRI image if a sensor is touched during the 12 s of procedure, or if there is loud, unfiltered background noise. In our observations, such artifacts were readily recognized by the image viewers. Automatic identification of such artifacts is being developed. Furthermore, mechanically ventilated patients encompass a distinctive class in which synchronization to other ventilator graphic displays (flow over time, pressure over time and tidal volume over time) would be advantageous.

Clinical directions for investigation were determined and studies are ongoing in the following areas: (1) repeatability and reliability of VRI in normal subjects; (2) determining VRI accuracy in assessing regional lung function in populations such as lung cancer and emphysema patients; (3) facilitating interventional pulmonology; (4) management of congestive heart failure patients; (5) management of lung transplant and lung volume reduction surgery patients; (6) accuracy in diagnosis and management of asthma; (7) management of chronic obstructive pulmonary disease patients; (8) ability to rule out lung pathology in outpatients with acute respiratory symptoms; (9) potential in providing bedside information for adjusting mechanical ventilation in critically ill patients; (10) ability to predict successful extubation; (11) utility for screening high-risk populations such as occupational patients.

Acknowledgements

VRI images and clinical data were provided by the following team of VRI investigators: R.P.D. and J.E.P. from the Division of Cardiovascular Disease and Critical Care Medicine, UMDNJ – Robert Wood Johnson Medical School at Camden, Cooper University Hospital, Camden, N.J., USA; Dr. Heinrich D. Becker from the Department of Interdisciplinary Endoscopy, Thoraxklinik at Heidelberg University, Heidelberg, Germany; Drs. Lea Bentur from the Pediatric Pulmonology Unit and Mordechai Iglu from the Pulmonary Division, Rambam Medical Center, Haifa, Israel; Dr. Ram Mor from the Department of Allergy and Pulmonary Diseases, Tel-Aviv Sourasky Medical Center, Tel Aviv, Israel.

Appendix 1

The VRI system includes N transducers (sensors) configured for attachment to an essentially planar region R on the individual's back. Positions in the region R are indicated by two-dimensional position vectors $x = (x^1, x^2)$ in a two-dimensional coordinate system defined in the planar region R . The i transducer, for $i = 1$ to N , is fixed at a position x_i in the region R and generates a signal, denoted herein by $p(x_i, t)$ indicative of pressure waves in the body arriving at x_i . The N signals $p(x_i, t)$ are processed by signal processing circuitry.

The average vibration energy $\tilde{P}(x_i, t_1, t_2)$ over a time interval from t_1 to t_2 is obtained at positions x_i of the sensors. The energy is calculated at each position of the sensors using equation (1). The energy at any location x is estimated using an interpolation method.

$$\tilde{P}(x_i, t_1, t_2) = \int_{t_1}^{t_2} P^2(x_i, t) dt, \quad (1)$$

where x_i is the position of the sensor.

The interpolation method is performed as follows: $\tilde{P}(x, t_1, t_2)$ at a position $x = (x^1, x^2)$ in the surface R using the algebraic expression in:

$$\tilde{P}(x, t_1, t_2) = \sum_{i=1}^N \tilde{P}(x_i, t_1, t_2) g(x, x_i, \sigma), \quad (2)$$

where x_i is the position of the sensor.

Where $g(x, x_i, \sigma)$ is a kernel satisfying:

$$\nabla^2 g = \frac{\partial g}{\partial \sigma} \quad (3)$$

$$\sum_{i=1}^N g(x, x_i, \sigma) \quad (4)$$

is approximately equal to 1 and where $x_i = (x_i^1, x_i^2)$ is the position of the i microphone and σ is a selectable parameter.

For example, the kernel:

$$g(x, x_i, \sigma) = \text{Exp}\left[-\frac{(x^1 - x_i^1 \sqrt{\sigma})^2}{2\sigma}\right] * \text{Exp}\left[-\frac{(x^2 - x_i^2 \sqrt{\sigma})^2}{2\sigma}\right] \quad (5)$$

may be used.

The VRI algorithm takes into consideration the distance between the sensors' centers. Lung parenchyma sound speed is estimated to be between 23 and 60 m/s, and lung solid components sound speed is estimated at approximately 1,500 m/s [9, 19, 20]. In order to ensure that the V-array sensors capture only the short wavelengths of the lung parenchyma, the distance between the V-array sensors was kept at $\lambda/2$ with a resolution of $\lambda/4$. A time interval can be divided into subintervals, and the average vibration energy \tilde{P} is determined over the region R for 2 or more of the subintervals. An image \tilde{P} for each of these subintervals may then be determined and displayed sequentially on the display device.

References

- 1 Elphick HE, Lancaster GA, Solis A, Majumdar A, Gupta R, Smyth RL: Validity and reliability of acoustic analysis of respiratory sounds in infants. *Arch Dis Child* 2004;89:1059–1063.
- 2 Murphy RL, Vyshedskiy A, Power-Charnitsky VA, Bana DS, Marinelli PM, Wong-Tse A, Paciej R: Automated lung sound analysis in patients with pneumonia. *Respir Care* 2004;49:1490–1497.
- 3 Earis JE, Cheetham BMG: Future perspectives for respiratory sound research. *Eur Respir Rev* 2000;10:641–646.
- 4 Stewart J: A measured breath: new techniques in pulmonary imaging and diagnosis. *CMAJ* 1996;154:847–850.
- 5 Earis JE, Cheetham BMG: Current methods used for computerized respiratory sound analysis. *Eur Respir Rev* 2000;10:586–590.
- 6 Pasterkamp H, Kraman SS, DeFrain PD, Wodicka GR: Measurement of respiratory acoustical signals: comparison of sensors. *Chest* 1993;104:1518–1525.
- 7 Pasterkamp H, Kraman SS, Wodicka GR: Respiratory sounds: advances beyond the stethoscope. *Am J Respir Crit Care Med* 1997;156:974–987.
- 8 Kompis M, Pasterkamp H, Wodicka GR: Acoustic imaging of the human chest. *Chest* 2001;120:1309–1321.
- 9 Charleston-Villalobos S, Cortes-Rubiano S, Gonzalez-Camarena R, Chi-Lem G, Aljama-Corrales T: Respiratory acoustic thoracic imaging (RATHI): assessing deterministic interpolation techniques. *Med Biol Eng Comput* 2004;42:618–626.
- 10 Sovijarvi ARA, Malmberg LP, Charbonneau G, Vanderschoot J, Dalmaso F, Sacco C, Rossi M, Earis JE: Characteristics of breath sounds and adventitious respiratory sounds. *Eur Respir Rev* 2000;10:591–596.
- 11 Ploy-Song-Sang Y, Martin RR, Ross WR, Loudon RG, Macklem PT: Breath sounds and regional ventilation. *Am Rev Respir Dis* 1977;116:187–199.
- 12 Leblanc P, Macklem PT, Ross WR: Breath sounds and distribution of pulmonary ventilation. *Am Rev Respir Dis* 1970;102:10–16.
- 13 O'Donnell DM, Kraman SS: Vesicular lung sound amplitude mapping by automated flow-gated phonopneumography. *J Appl Physiol* 1982;53:603–609.
- 14 Ploy-Song-Sang Y, Macklem PT, Ross WR: Distribution of regional ventilation measured by breath sounds. *Am Rev Respir Dis* 1978;117:657–664.
- 15 Pasterkamp H, Consunji-Araneta R, Oh Y, Holbrow J: Chest surface mapping of lung sounds during methacholine challenge. *Pediatr Pulmonol* 1997;23:21–30.
- 16 Dosani R, Kraman SS: Lung sound intensity variability in normal men: a contour phonopneumographic study. *Chest* 1983;83:628–631.
- 17 Pasterkamp H, Patel S, Wodicka GR: Asymmetry of respiratory sounds and thoracic transmission. *Med Biol Eng Comput* 1997;35:103–106.
- 18 Anderson K, Aitken S, Carter R, MacLeod JE, Moran F: Variation of breath sound and airway caliber induced by histamine challenge. *Am Rev Respir Dis* 1990;141:1147–1150.
- 19 Schreur HJ, Diamant Z, Vanderschoot J, Zwinderman AH, Dijkman JH, Sterk PJ: Lung sounds during allergen-induced asthmatic responses in patients with asthma. *Am J Respir Crit Care Med* 1996;153:1474–1480.
- 20 Vannuccini L, Earis JE, Helisto P, Cheetham BMJ, Rossi M, Sovijarvi ARA, Vanderschoot J: Capturing and preprocessing of respiratory sounds. *Eur Respir Rev* 2000;10:616–620.
- 21 Bellemare J-F, Cordeau M-P, Leblanc P, Bellemare F: Thoracic dimensions at maximum lung inflation in normal subjects and in patients with obstructive and restrictive lung diseases. *Chest* 2001;119:376–386.
- 22 Rice DA: Transmission of lung sounds. *Semin Respir Med* 1985;6:166–170.
- 23 Sureshbabu W, Mawlawi O: PET/CT imaging artifacts. *J Nucl Med Technol* 2005;33:156–161.
- 24 Ploysongsang Y, Iyer VK, Ramamoorthy PA: Inspiratory and expiratory vesicular breath sounds. *Respiration* 1990;57:313–317.
- 25 Fiz JA, Jane R, Izquierdo J, Homs A, Garcia MA, Gomez R, Monso E, Morera J: Analysis of forced wheezes in asthma patients. *Respiration* 2006;73:55–60.
- 26 Bohadana AB, Kopferschmitt-Kubler MC, Pauli G: Breath sound intensity in patients with airway provocation challenge test positive by spirometry but negative for wheezing: a preliminary report. *Respiration* 1994;61:274–279.